A GABOR FEATURE FUSION FRAMEWORK FOR HYPERSPECTRAL IMAGERY CLASSIFICATION

Sen Jia[†]*, Bin Deng*[†]*, Huimin Xie*[†] *and Lin Deng*[‡]

[†]College of Computer Science and Software Engineering, Shenzhen University, China
[‡]College of Information Engineering, Shenzhen University, China

ABSTRACT

Hyperspectral imagery acquired by a hyperspectral sensor contains hundreds of narrow contiguous spectral bands, providing the opportunity to identify the various materials present on the surface. Due to the three-dimensional (3D) nature of hyperspectral data, 3D filters that could extract joint spatial-spectral features have been recently considered in the literature. In this paper, after the 3D Gabor features with certain orientations have been extracted from the raw hyperspectral image data, both the Gabor magnitude and phase features have been used for hyperspectral imagery classification, which is named as Gabor-MP. Specifically, the confidence score of each test sample is computed by support vector machine for each Gabor magnitude feature cube, while the Hamming distance is calculated based on the quadrant bit coding of each Gabor phase feature cube. Then the label of the test sample is identified by simple calculation between the confidence scores and Hamming distance values. Experimental results on two real hyperspectral data have demonstrated the effectiveness of the proposed Gabor feature fusion framework for hyperspectral imagery classification.

***Index Terms*—** Hyperspectral imagery classification, feature fusion

1. INTRODUCTION

In last two decades, hyperspectral imagery classification has been extensively studied, in which the major challenge is the large number of spectral features and limited training samples (due to the difficulty and expense of manual labeling) [1, 2]. Fortunately, spatial structure information of materials, which means the adjacent pixels belong to the same class with a high probability, is a valuable complement to the spectral information [3]. Due to the three-dimensional (3D) nature of hyperspectral data, it is more desirable to extract joint spatial-spectral features for classification.

This work was supported in part by the National Natural Science Foundation of China under Grant 61671307, in part by the Guangdong Special Support Program of Top-notch Young Professionals under Grant 2015TQ01X238, and in part by the Shenzhen Scientific Research and Development Funding Program under Grant JCYJ20160422093647889 and Grant SGLH20150206152559032.

3D Gabor wavelet has been introduced for hyperspectral image classification, which can achieve optimal joint time/frequency and space/frequency resolutions for signal analysis [4, 5]. Concretely, a set of 3D complex Gabor wavelet filters with multiple frequencies and orientations has been predefined, which are convolved with the original hyperspectral image data to extract joint spatial-spectral features. The magnitude of the response at each pixel is then used for feature representation, while the phase information of Gabor features are directly discarded. A feature selection process has been further developed to reduce the redundancy among the obtained high dimensional features [6, 7]. However, it is not a trivial task to decide which features should be picked out from the obtained ones.

Recent advances have revealed that the Gabor phase has sufficient discriminative ability for classification, as long as the phase information has been encoded properly [8]. In this paper, after the 3D Gabor features with certain orientations have been extracted from the raw hyperspectral image data, both the Gabor magnitude and phase features have been used for hyperspectral imagery classification, thus the proposed method is named as Gabor-MP. Specifically, the confidence score of each test sample is computed by support vector machine for each Gabor magnitude feature cube, while the Hamming distance between the test sample and every class is calculated based on the quadrant bit coding of each Gabor phase feature cube. The confidence scores and Hamming distance values of all the Gabor magnitude and phase features are respectively summed up, and the test sample is assigned to the class with the maximal value of the substraction of the two terms. Figure 1 illustrates the schematic diagram of the proposed strategy. Experimental results on two real hyperspectral data have demonstrated the effectiveness of the proposed magnitude-phase-combined approach for hyperspectral imagery classification.

The rest of this paper is organized as follows. In Section 2, we introduce the basic notations and briefly describe the related works. Section 3 present the proposed Gabor feature fusion framework. Afterward, the experimental results on two real hyperspectral remote sensing data are reported in Section 4. Finally, conclusions are given in Section 5.

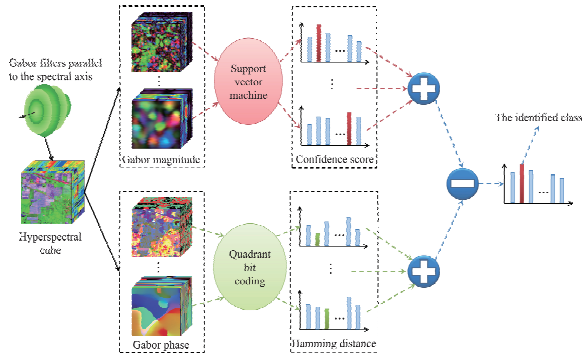

Fig. 1. System block diagram of the proposed Gabor-MP framework for hyperspectral image classification.

2. GABOR WAVELET TRANSFORM

Let $\mathbf{R} \in \mathbb{R}^{X \times Y \times B}$ denote the hyperspectral image cube that contains two spatial dimensions X and Y (pixels) and one spectral dimension B (wavelength). In frequency domain (u, v, w), let φ and θ respectively denote the angles of the frequency vector f with w-axis and $u-v$ plane, a 3D Gabor wavelet for a certain pixel at the spatial-spectral position (x, y, b) can be designed as:

$$\Psi_{f,\varphi,\theta}(x,y,b) = \frac{1}{(2\pi)^{2/3}\sigma^3} \exp(j2\pi(xu+yv+bw)) \times \exp\left(-\frac{x^2+y^2+b^2}{2\sigma^2}\right) \quad (1)$$

$$u = f\sin\varphi\cos\theta, v = f\sin\varphi\sin\theta, w = f\cos\varphi$$

where f is the central frequency of the sinusoidal plane wave, and σ is the width of Gaussian envelope in (x, y, b) domain.

Due to the sensitivity of phase information to the varying positions, in this paper, only the Gabor features extracted by Gabor filters with the direction parallel to the spectral axis, that is, both the parameters θ and φ in equation (1) are $\pi/2$, are used for classification. This is expected since the Gabor filters that are parallel to the spectral axis is in accordance with the data structure of hyperspectral imagery (as displayed in Figure 1), so each pixel can be well characterized by the extracted rich information. Besides, the frequency f takes the values of $[0.5, 0.25, 0.125, 0.0625]$, and the used Gabor filters is expressed as $\Psi_k, k = 1, \ldots, 4$ for simplicity.

For a certain Gabor wavelet Ψ_k, the coefficient $\mathbf{G}_k(x, y, b) = (\mathbf{R} \otimes \Psi_k)(x, y, b)$ represents the local signal change information around location (x, y) at spectral band b, where $\otimes$ is the convolution operation. At location (x, y), the Gabor responses at different bands, i.e. $\mathbf{G}_k(x, y) = [\mathbf{G}_k(x, y, 1), \mathbf{G}_k(x, y, 2), \ldots, \mathbf{G}_k(x, y, B)]$, contain important information about the signal variances with centre frequency f_k at space, spectrum and joint spatial/spectral domains. As the Gabor wavelet Ψ_k is complex, the convolution coefficient at (x, y, b) can be represented by magnitude $\mathbf{M}_k(x, y, b)$ and phase $\mathbf{P}_k(x, y, b)$, respectively:

$$\mathbf{M}_k(x,y,b) = \sqrt{\mathrm{Re}(\mathbf{G}_k(x,y,b))^2 + \mathrm{Im}(\mathbf{G}_k(x,y,b))^2} \quad (2)$$

$$\mathbf{P}_k(x,y,b) = \arg\tan\frac{\mathrm{Im}(\mathbf{G}_k(x,y,b))}{\mathrm{Re}(\mathbf{G}_k(x,y,b))} \quad (3)$$

where Im and Re operations get the imaginary and real parts of the complex coefficient, respectively. It is worth to mention that each Gabor magnitude feature cube has the same dimensions as the original hyperspectral image. Similarly, each Gabor phase feature cube has the same size.

3. THE PROPOSED APPROACH

In order to effectively fuse the Gabor magnitude and phase features, different classification strategies have been adopted. Specifically, for each Gabor magnitude feature cube, support vector machine (SVM) classifier is used for classification. Here the LIBSVM software package is adopted, in which the radial basis function (RBF) kernel and one-against-one scheme are employed for multi-class classification [9]. Suppose there are P significant materials existing in the scene, $P \times (P-1)$ classifiers can be thus constructed by SVM for each test sample. The confidence score of the test sample to each class for the k-th Gabor magnitude feature cube is computed by:

$$\mathcal{S}_k^p = \frac{n_p}{P}, \quad p = 1, \ldots, P \quad (4)$$

where n_p is the number of non-zero entries in the p-th row. Clearly, the range of $\mathcal{S}_k^p$ is between 0 and 1. The larger the confidence score $\mathcal{S}_k^p$, the higher probability the test sample belonging to the p-th class.

Alternatively, concerning each Gabor phase feature cube, a typical phase-quadrant demodulation coding method, called Quadrant Bit Coding (QBC) [10], is applied to increase the stability of Gabor phase features, which encodes the phase according to the quadrant it belongs to. More precisely, each pixel in $\mathbf{P}_k(x, y, b), k = 1, \ldots, 4$ is encoded to two bits by the following rules:

$$\mathbf{Q}_k^{Re}(x,y,b) = \begin{cases} 1 & \text{if} \quad \mathbf{P}_k(x,y,b) \in \{\mathrm{I}, \mathrm{IV}\} \\ 0 & \text{if} \quad \mathbf{P}_k(x,y,b) \in \{\mathrm{II}, \mathrm{III}\} \end{cases} \quad (5)$$

$$\mathbf{Q}_k^{Im}(x,y,b) = \begin{cases} 1 & \text{if} \quad \mathbf{P}_k(x,y,b) \in \{\mathrm{I}, \mathrm{II}\} \\ 0 & \text{if} \quad \mathbf{P}_k(x,y,b) \in \{\mathrm{III}, \mathrm{IV}\} \end{cases} \quad (6)$$

Obviously, the same feature can be obtained within every 90 degree $((0°, 90°], (90°, 180°], (180°, 270°], (270°, 360°])$.

After the Gabor phase of the hyperspectral images has been encoded by the QBC strategy, eight binary feature cubes, $\mathbf{Q}_k^{Re}$ and $\mathbf{Q}_k^{Im}, k = 1, \ldots, 4$, have been obtained. For any test sample $\mathbf{t}$ with spatial position (x_{tt}, y_{tt}), a normalized Hamming distance is applied to measure the material similarity. Concretely, assuming the spatial axes of any training sample $\mathbf{s}$ in the training set $\mathbf{A}$ are (x_{tr}, y_{tr}), the normalized Hamming distance between the test sample $\mathbf{t}$ and the training sample $\mathbf{s}$ is computed by

$$h_k(\mathbf{t}, \mathbf{s}) = \frac{\sum_{b=1}^{B}(bit_k^{Re} + bit_k^{Im})}{2 \times B} \tag{7}$$

$$\begin{aligned} bit_k^{Re} &= \mathbf{Q}_k^{Re}(x_{tt}, y_{tt}, b) \oplus \mathbf{Q}_k^{Re}(x_{tr}, y_{tr}, b) \\ bit_k^{Im} &= \mathbf{Q}_i^{Im}(x_{tt}, y_{tt}, b) \oplus \mathbf{Q}_k^{Im}(x_{tr}, y_{tr}, b) \end{aligned} \tag{8}$$

where $\oplus$ is the bit XOR operator, i.e., the result is equal to zero if and only if the two bits, $\mathbf{Q}_i(x_{tt}, y_{tt}, b)$, are equal to $\mathbf{Q}_i(x_{tr}, y_{tr}, b)$. Similarly, $h_k(\mathbf{t}, \mathbf{s})$ is between 0 and 1. The smaller the Hamming distance, the more similar between the test sample and the training sample. The Hamming distance between test sample t and the p-th class is calculated as:

$$\mathcal{H}_k^p = \min_{\mathbf{A}_i \in p} h_k(\mathbf{t}, \mathbf{A}_i) \tag{9}$$

At last, the confidence scores and Hamming distance respectively obtained from the Gabor magnitude and phase features are combined by the following formula:

$$\mathcal{D}^p = \sum_{k=1}^{4}(\mathcal{S}_k^p - \mathcal{H}_k^p), \quad p = 1, \ldots, P \tag{10}$$

That is, the test sample $\mathbf{t}$ is assigned to class p if $\mathcal{D}^p$ is the largest among all classes.

4. EXPERIMENTAL RESULTS

Two real hyperspectral image data sets are evaluated. The first one is the commonly-used Indian pines data set acquired by the AVIRIS instrument over the agricultural area of Northwestern Indiana in 1992, which has spatial dimension of 145×145 and 224 spectral bands. The spatial resolution of the data is 20m per pixel. After discarding four zero bands and 35 lower signal-to-noise ratio (SNR) bands affected by atmospheric absorption, 185 channels are preserved. The data set contains 10366 labeled pixels and 16 ground-truth classes, most of which are different types of crops.

The second one was acquired by the ROSIS-03 sensor over the university of Pavia, Italy with 115 spectral bands. After removing the 12 noisiest bands, the remaining 103 channels are processed. Each band image is of size 610×340 and the spatial resolution is 1.3m per pixel. There are 42776 labeled samples in total, and nine classes of interest are considered. The ground truth are presented in Figure 2 and 3. Detailed information about the data can be found in [11].

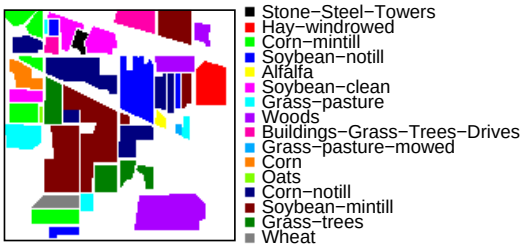

Fig. 2. Ground-truth map of the Indian Pines data set (sixteen land cover classes).

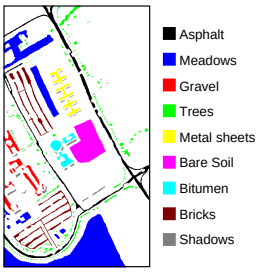

Fig. 3. Ground-truth map of the Pavia University data set (nine land cover classes).

Five methods are compared with the proposed Gabor-MP approach, i.e., Gabor magnitude feature-based SVM with radial basis function (RBF) kernel and SRC classifiers [5] (abbreviated as FM-RBFSVM and FM-SRC, respectively), Gabor phase feature-based coding and matching (abbreviated as Gabor-P), and two state-of-the-art spectral-spatial-integrated classification techniques, including multiple feature (extracted from linear and nonlinear transformations) learning-based classification (MFL) [12] and local binary patterns-based extreme learning machine (LBP-ELM) [13]. For SVM, one-against-one scheme was used for multi-class classification and its parameters are estimated by cross validation. For SRC, the Homotopy method is used to recover the sparse signals [14]. For MFL and LBP-ELM, the parameters are set the same as their original papers.

As far as the small sample size problem is mainly concerned in this paper, the performance of six compared methods is evaluated with different sample sizes: fixed number of the provided labeled samples is randomly picked out from each class to constitute the training set, and the remaining samples are then used for evaluation. Each experiment is repeated ten times with different training sets to make the comparison fair, and both the mean accuracies and standard deviation are reported. Concerning the evaluation metrics, overall accuracy (OA) and kappa coefficient (κ) are adopted to quantify the classification performance. Specifically, OA is

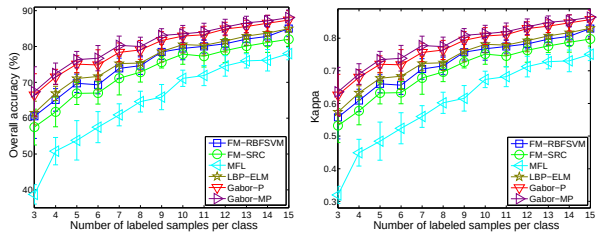

(a) (b)

Fig. 4. Indian Pines data: (a) Overall accuracy and (b) Kappa as functions of the number of labeled samples per class.

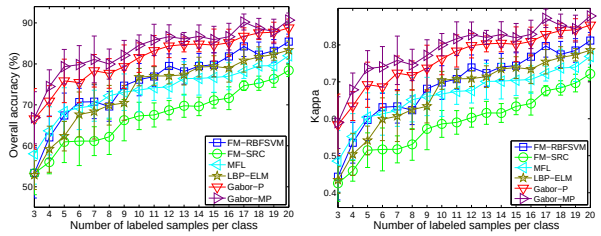

(a) (b)

Fig. 5. Pavia University data: (a) Overall accuracy and (b) Kappa as functions of the number of labeled samples per class.

computed by dividing the sum of the correctly classified samples by the total number of test samples, while κ is computed by accounting for all elements in the confusion matrix [15]. Clearly, higher values of the two metrics correspond to better classification performance.

For the Indian Pines hyperspectral data, the classification accuracy (OA) and kappa coefficient measure as functions of the number of training samples per class $(3, 4, \ldots, 15)$ is conducted, as displayed in Figure 4. From the figure we can see, as expected, the increase of the training size has a favorable effect in the performance of all the six methods. The results of MFL are lower than the other five methods. Meanwhile, the performance of the two Gabor magnitude based methods (FM-RBFSVM and FM-SRC) and LBP-ELM are comparable, while our Gabor-MP method is better than Gabor-P and consistently provides the best results, demonstrating the effectiveness of the proposed approach. In particular, when the training size is very small, the differences between the algorithms are apparent.

Alternatively, considering the Pavia University hyperspectral data, Figure 5 illustrates the OA and kappa coefficient as functions of the training size for the samples per class $(3, 4, \ldots, 20)$. It can be seen from the figure that the classification accuracies improve as the number of the training samples increases. As before, the results obtained by our Gabor-MP method are more accurate than those of the other five ones. This is in line with our previous experiments, where it can be observed that Gabor-MP is a better alternative than the other five methods.

5. CONCLUSION

In this paper, we have developed a Gabor feature fusion framework, called Gabor-MP, for hyperspectral image classification. We firstly introduced support vector machine with the one-against-one strategy to obtain the decision matrix from each Gabor magnitude feature cube, which is then transformed into confidence score of every class to boost the discriminative capability. Secondly, the Gabor phase cube features are coded by the QBC scheme, and the Hamming distance measure is used to evaluate the class similarity. Finally, both the confidence score and the Hamming distance are combined together to accomplish the classification task. Experimental results on two real hyperspectral data set have demonstrated the superiority of the proposed algorithm over several state-of-the-art methods.

References

[1] A. Plaza, Jon Atli Benediktsson, J. Boardman, J. Brazile, L. Bruzzone, G. Camps-Vails, J. Chanussot, M. Fauvel, P. Gamba, A. Gualtieri, M. Marconcinie, J. C. Tilton, and G. Trianni, "Recent advances in techniques for hyperspectral image processing," *Remote Sens. Environ.*, vol. 113, pp. 110–122, Sep. 2009.

[2] J. M. Bioucas-Dias, A. Plaza, G. Camps-Valls, P. Scheunders, N. M. Nasrabadi, and J. Chanussot, "Hyperspectral remote sensing data analysis and future challenges," *IEEE Geosci. Remote Sens. Mag.*, vol. 1, no. 2, pp. 6–36, 2013.

[3] M. Fauvel, Y. Tarabalka, Jon Atli Benediktsson, J. Chanussot, and J. C. Tilton, "Advances in spectral-spatial classification of hyperspectral images," *Proc. IEEE*, vol. 101, no. 3, pp. 652–675, Mar. 2013.

[4] D. Gabor, "Theory of communication. part 1: The analysis of information," *J. Inst. Elect. Eng. III, Radio Commun. Eng.*, vol. 93, no. 26, pp. 429–457, 1946.

[5] L. Shen and S. Jia, "Three-dimensional Gabor wavelets for pixel-based hyperspectral imagery classification," *IEEE Trans. Geosci. Remote Sens.*, vol. 49, no. 12, pp. 5039–5046, Dec. 2011.

[6] S. Jia, L. Shen, and Q. Li, "Gabor feature-based collaborative representation for hyperspectral imagery classification," *IEEE Trans. Geosci. Remote Sens.*, vol. 53, no. 2, pp. 1118–1129, Feb. 2015.

[7] S. Jia, J. Hu, Y. Xie, L. Shen, X. Jia, and Q. Li, "Gabor cube selection based multitask joint sparse representation for hyperspectral image classification," *IEEE Trans. Geosci. Remote Sens.*, vol. 54, no. 6, pp. 3174–3187, Jun. 2016.

[8] Wenchao Zhang, Shiguang Shan, Laiyun Qing, Xilin Chen, and Wen Gao, "Are Gabor phases really useless for face recognition?," *Pattern Anal. Appl.*, vol. 12, no. 3, pp. 301–307, 2009.

[9] Chih-Chung Chang and Chih-Jen Lin, "LIBSVM: a library for support vector machines," *ACM Trans. Intel. Syst. Tec.*, vol. 2, no. 3, pp. 1–27, 2011.

[10] John G Daugman, "High confidence visual recognition of persons by a test of statistical independence," *IEEE Trans. Pattern Anal. Mach. Intell.*, vol. 15, no. 11, pp. 1148–1161, 1993.

[11] Sen Jia, Yao Xie, Guihua Tang, and Jiasong Zhu, "Spatial-spectral-combined sparse representation-based classification for hyperspectral imagery," *Soft Comput.*, vol. 20, no. 12, pp. 4659–4668, 2016.

[12] Jun Li, Xin Huang, P. Gamba, J.M. Bioucas-Dias, Liangpei Zhang, Jon Atli Benediktsson, and A. Plaza, "Multiple feature learning for hyperspectral image classification," *IEEE Trans. Geosci. Remote Sens.*, vol. 53, no. 3, pp. 1592–1606, Mar. 2015.

[13] Wei Li, Chen Chen, Hongjun Su, and Qian Du, "Local binary patterns and extreme learning machine for hyperspectral imagery classification," *IEEE Trans. Geosci. Remote Sens.*, vol. 53, no. 7, pp. 3681–3693, Jul. 2015.

[14] S. Asif, *Dynamic compressive sensing: Sparse recovery of streaming signals and video*, Ph.D. thesis, Georgia Institute of Technology, 2013.

[15] John A Richards, *Remote sensing digital image analysis: an introduction*, Springer, 2013.